On Maximum Enstrophy Growth in a Hydrodynamic System

Diego Ayala and Bartosz Protas

Department of Mathematics & Statistics,
McMaster University, Hamilton, Ontario, Canada

July 4, 2011

Abstract

Enstrophy $\mathcal{E}$ plays an important role in the study of regularity of solutions to the three–dimensional Navier–Stokes equation. The best estimates for its growth available to–date do not rule out the possibility of enstrophy becoming unbounded in finite time which would indicate loss of regularity of solutions. It is therefore interesting to investigate sharpness of such finite–time bounds for enstrophy growth. We consider this question in the context of Burgers equation which is used as a "toy model". The problem of saturation of finite–time estimates for the enstrophy growth is stated as a PDE–constrained optimization problem

$$\max_{\phi}[\mathcal{E}(T)-\mathcal{E}(0)] \quad \text{subject to} \quad \mathcal{E}(0)=\mathcal{E}_0,$$

where the control variable ϕ represents the initial condition, which is solved numerically using an adjoint–based gradient method for a wide range of time windows T and initial enstrophies $\mathcal{E}_0$. We show that this optimization problem admits a discrete family of maximizers parameterized by the wavenumber m whose members are rescaled copies of the fundamental maximizer corresponding to $m=1$. It is found that the maximum enstrophy growth in finite time scales with the initial enstrophy as $\mathcal{E}_0^{\alpha}$ where $\alpha \approx 3/2$. The exponent is smaller than $\alpha=3$ predicted by analytic means, therefore suggesting possible lack of sharpness of analytical estimates.

Keywords: Enstrophy Growth; Burgers Equation; Optimization; Estimates; Blow–up Problem

1 Introduction

This investigation is motivated by an open question of mathematical fluid mechanics concerning the global–in–time existence of solutions of the three–dimensional (3D) Navier–Stokes system corresponding to arbitrary smooth initial data [1]. While the situation in regard to two–dimensional (2D) flows is quite satisfactory, i.e., smooth solutions corresponding to smooth initial data with arbitrary size are guaranteed to exist globally in time, for 3D flows only the existence of suitable weak solutions has been established for arbitrary times [2]. Since an analogous result is not available for strong (classical) solutions in 3D, the possibility that such solutions may lose their regularity in finite time, resulting in the so–called "blow–up", cannot be ruled out. If starting from smooth initial data the Navier–Stokes equation should lead in a finite time to the formation of singularities, then this would undermine the validity of this equation as a model of the flows of viscous incompressible fluids. The importance of this problem has been recognized by the Clay Mathematics Institute which has identified this problem as one the "Millennium Challenges" for the mathematics community [3], offering a suitable monetary prize for its resolution. The current state of the mathematical theory relevant to this problem is reviewed in the monographs by Constantin and Foias [4], Doering and Gibbon [5] and Temam [6]. We add that analogous open questions concerning the regularity of solutions in 3D pertain to the inviscid Euler equation [7, 8].

One approach to the problem relies on the fact, established in [9], that the velocity field $\mathbf{u}(t,\mathbf{x}) \,:\, \mathbb{R}^+ \times \mathbb{R}^3 \to \mathbb{R}^3$ remains smooth as long as the *enstrophy*, defined as

$$\mathcal{E}(t) \triangleq \frac{1}{2}\int_\Omega |\boldsymbol{\nabla} \times \mathbf{u}(t,\mathbf{x})|^2 \, d\Omega, \tag{1}$$

where Ω is the flow domain and "$\triangleq$" means "equal to by definition", remains bounded. We note that for flows defined, as is often the case for this problem, on domains with periodic boundary conditions in all three directions, enstrophy (1) can be expressed in terms of the velocity gradient $\boldsymbol{\nabla}\mathbf{u}$ as $\mathcal{E}(t) = (1/2)\|\boldsymbol{\nabla} u(t,\cdot)\|^2_{L^2(\Omega)}$, where $\|\cdot\|_{L^2(\Omega)}$ denotes the L_2 norm of functions defined on Ω. The maximum values that the enstrophy can attain over a time interval are determined by its rate of growth $d\mathcal{E}(t)/dt$, and the best estimate available to–date for this quantity is [5]

$$\frac{d\mathcal{E}(t)}{dt} \leq \frac{27C^3}{32\nu^3}\mathcal{E}(t)^3, \tag{2}$$

where $C = 2\sqrt{2/\pi}$ and ν is the kinematic viscosity of the fluid. Details of the derivation of (2) can be found, for example, in [10]. It should be remarked that the incompressibility condition $\boldsymbol{\nabla}\cdot\mathbf{u} = 0$ is not explicitly taken into account in the derivation of (2). Instantaneous estimate (2) was recently found to be sharp up to a constant prefactor by

Lu and Doering [10, 11], however, sharpness of this estimate over finite time windows is an open problem. We observe that integrating this estimate in time indicates a blow–up of the enstrophy bound occurring at the time $t_0 = \frac{16\nu^3}{27C^3\mathcal{E}_0^2}$, where $\mathcal{E}_0$ is the initial value of the enstrophy. Therefore, establishing whether or not estimate (2) is sharp over finite time windows can have important consequences for the resolution of the regularity problem.

One possible approach to obtain insights concerning sharpness of estimate (2) for finite times is to compute numerically solutions characterized by large growth of enstrophy to see whether this growth saturates the estimate. In fact, such investigations were first undertaken in the context of the Euler equation, and in his pioneering work Kerr [12] predicted a finite–time blow–up. These calculations were later revisited, together with several other configurations, by Hou and coworkers [13] offering no support for finite–time blow–up in the Euler equation. In the context of computational studies of the blow–up problem for the Navier–Stokes system we should also mention the work of Pelz [14], and Ohkitani & Constantin [15]. Another related research direction involves the study of complex–valued extensions of the Euler and Navier–Stokes equations. The idea is that solutions to the equations which are real–analytic functions of the space variables possess singularities in the complex plane, and the distance from the real axis to the nearest singularity, referred to as the width of the analyticity strip [16], further characterizes the smoothness of the solution. Therefore, migration of such complex–plane singularities towards the real line might be a signature of an approaching blow–up. In the context of this approach we only mention recent studies [17, 18], and refer the reader to the references quoted therein for further details. **On the other hand, modifications of the hydrodynamic evolution equations which lead to solutions in the form of entire functions of the space variables were studied in [19].** It should be emphasized that in all the computational investigations of the blow–up problem mentioned above the initial conditions considered as possible candidates for blow–up were postulated in a rather ad–hoc manner.

A fundamentally different approach to this problem originated with the work of Lu and Doering [10, 11] who framed the question about sharpness of estimate (2) as an optimization problem. More specifically, they solved computationally, using a gradient descent method, a family of optimization problems in the following form

$$\begin{aligned} &\max_{\mathbf{u}\in\mathbf{H^1}(\Omega),\, \boldsymbol{\nabla}\cdot\mathbf{u}=0} \frac{d\mathcal{E}}{dt}, \\ &\text{subject to } \mathcal{E} = \mathcal{E}_0, \end{aligned} \tag{3}$$

where $\frac{d\mathcal{E}}{dt}$, the instantaneous rate of growth of enstrophy, can be expressed in terms of vector field $\mathbf{u}$ using the Navier–Stokes equation, and $\mathbf{H^1}(\Omega)$ denotes the Sobolev space of vector–valued functions with square–integrable gradients. Solutions of problem (3) are

thus solenoidal vector fields $\mathbf{u}$ with prescribed enstrophy $\mathcal{E}_0$ which achieve the highest possible enstrophy growth. Solving problem (3) numerically for a range of different values of $\mathcal{E}_0$, Lu and Doering were able to find a family of vector fields $\mathbf{u}$ saturating estimate (2) up to a constant prefactor, i.e., whose rate of enstrophy growth scales with the third power of $\mathcal{E}_0$ [10, 11]. However, since optimization problem (3) is "instantaneous", i.e., formulated at a single instant of time, it is not obvious whether using the optimal solutions of problem (3) as initial conditions for the Navier–Stokes system, the rate of growth of enstrophy allowed by estimate (2) would be sustained over some time leading to eventual blow–up in finite time.

In order to obtain some insights regarding sharpness of estimate (2) over finite time windows, one would need to solve an optimization problem analogous to (3), but formulated on a finite time interval $[0, T]$ for some $T > 0$, and this is a long–term objective of the present research effort. Needless to say, solution of such an optimization problem, in which the full Navier–Stokes equation appears as the constraint, is in fact a formidable computational task. In this investigation we are concerned with a closely related, albeit much simpler, problem in which the finite–time optimization problem is posed for a one–dimensional (1D) model problem, namely the viscous Burgers equation. While the existence theory of classical solutions to Burgers equation is complete and guarantees the global–in–time existence of smooth solutions from smooth initial data of arbitrary size [20], it is possible to derive estimates for the growth of enstrophy similar to (2) and questions concerning their sharpness are still quite relevant. To be precise, the best available estimate for the instantaneous rate of growth of enstrophy in viscous Burgers equation is [11]

$$\frac{d\mathcal{E}(t)}{dt} \leq \frac{3}{2}\left(\frac{1}{\pi^2\nu}\right)^{1/3}\mathcal{E}(t)^{5/3} \tag{4}$$

which, after integrating with respect to time over the interval $[0, T]$, leads to the following upper bound on the finite–time maximum of enstrophy corresponding to the initial enstrophy $\mathcal{E}_0$ [21, **see Appendix A in the present work for derivation**]

$$\max_{t\in[0,T]}\mathcal{E}(t) \leq \left[\mathcal{E}_0^{1/3} + \left(\frac{L}{4}\right)^2\left(\frac{1}{\pi^2\nu}\right)^{4/3}\mathcal{E}_0\right]^3 \underset{\mathcal{E}_0\to\infty}{\longrightarrow} \left(\frac{L}{4}\right)^6\left(\frac{1}{\pi^2\nu}\right)^4\mathcal{E}_0^3, \tag{5}$$

where L is the size of the domain. Assessing the sharpness of estimate (5), which has been obtained using techniques commonly applied to the 3D Navier–Stokes problem, is the main goal of this investigation. The structure of this paper is as follows: in the next Section we present a formal statement of the optimization problem and in the following Section we describe a computational approach to the solution of this problem; computational results are presented in Section 4, whereas discussion and conclusions are deferred to Section 5; in Appendix A we present some details concerning the derivation of

estimate (5), whereas in Appendix B some additional information is provided as regards the adjoint–based method used to solve the optimization problem.

2 Saturation of Enstrophy Estimates for Burgers Equation

We consider viscous Burgers equation on 1D periodic domain $\Omega \triangleq [0,1]$, **i.e., we set** $L = 1$ **in** (5)**,**

$$\frac{\partial u}{\partial t} + u\frac{\partial u}{\partial x} - \nu\frac{\partial^2 u}{\partial x^2} = 0 \qquad \text{in } (0,T]\times\Omega, \tag{6a}$$

$$u(x) = \phi(x) \qquad \text{in } \Omega \text{ at } t = 0, \tag{6b}$$

$$\text{Periodic BC} \qquad \text{for } t > 0, \tag{6c}$$

where "BC" stands for "boundary conditions", $\phi(x)$ denotes the initial data and the enstrophy is now defined as

$$\mathcal{E}(t) = \frac{1}{2}\int_0^1 \left|\frac{\partial u(t,x)}{\partial x}\right|^2 dx. \tag{7}$$

Sharpness of estimate (4) was also addressed by Lu and Doering [10, 11] who considered the following instantaneous optimization problem

$$\begin{aligned} &\max_{u\in H^1(\Omega)} \frac{d\mathcal{E}}{dt}, \\ &\text{subject to } \mathcal{E} = \mathcal{E}_0, \end{aligned} \tag{8}$$

where $H^1(\Omega)$ denotes the Sobolev space of scalar–valued functions periodic on Ω with square–integrable derivatives, and the rate of growth of enstrophy can be expressed in terms of the field u as

$$\frac{d\mathcal{E}}{dt} = -\nu\left\|\frac{\partial^2 u}{\partial x^2}\right\|_{L_2}^2 + \frac{1}{2}\int_0^1 \left(\frac{\partial u}{\partial x}\right)^3 dx. \tag{9}$$

Remarkably, Lu and Doering [10, 11] were able to determine the maximizer $\tilde{u}$ of problem (8) in closed form, namely

$$\tilde{u}(x) = \int v(x')\,dx', \qquad \text{where} \tag{10a}$$

$$v(x) = (\beta_2 - \beta_3)\,\mathrm{sn}^2\left(\sqrt{\frac{\beta_1-\beta_3}{8\nu}}x\right) + \beta_3, \tag{10b}$$

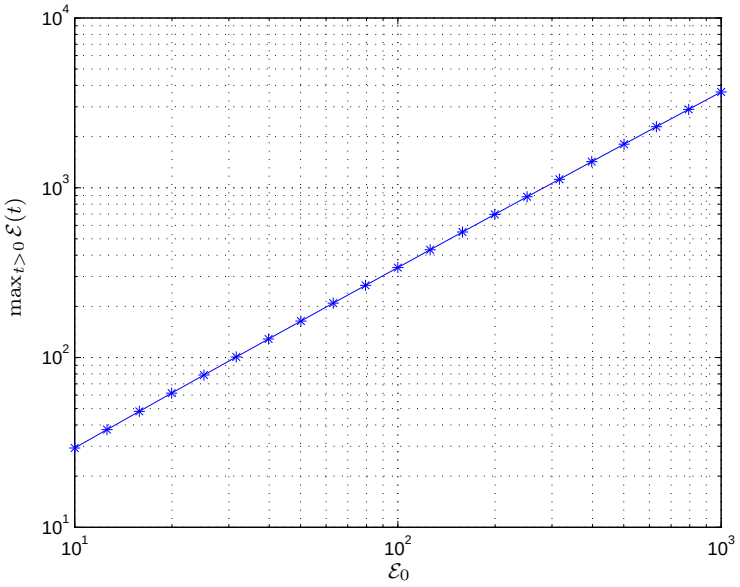

Figure 1: Scaling of $\max_{t>0} \mathcal{E}(t)$ with respect to $\mathcal{E}_0$ for solutions of initial–value problem (6) with instantaneously optimal initial data (10). **Power law** (14) **which describes this relation has the exponent** $\alpha = 1.048 \pm 0.018$**.**

in which $\mathrm{sn}(\cdot)$ is the elliptic function of the first kind and the constants β_1, β_2 and β_3 are given by

$$\beta_1 = 32\nu K(m)E(m), \tag{11a}$$

$$\beta_2 = 32\nu K(m)\left(E(m) - (1-m)K(m)\right), \tag{11b}$$

$$\beta_3 = 32\nu K(m)\left(E(m) - K(m)\right). \tag{11c}$$

The functions $K(m)$ and $E(m)$ in equations (11) are the complete elliptic integrals of the first and second kind, respectively, whereas the parameter $m \in (0,1)$ satisfies the equation

$$\frac{1024\nu^2}{3}K^3\left[(2+m)K - 2(1+m)E\right] - 1024\nu^2K^2\left(K-E\right)^2 = 2\mathcal{E}_0, \tag{12}$$

where the dependence of K and E on m has been omitted for brevity.

For large values of the enstrophy $\mathcal{E}_0$ the rate of growth of enstrophy exhibited by the field $\tilde{u}(x)$ was found to scale as

$$\frac{d\mathcal{E}}{dt} \approx \frac{0.2476}{\nu^{1/3}}\mathcal{E}_0^{5/3} \tag{13}$$

confirming that instantaneous estimate (4) is in fact sharp up to a prefactor [10, 11]. An important question is whether the time–dependent solutions starting from instantaneous optimizers of problem (8) can actually saturate finite–time bound (5). Solving initial–value problem (6) with such instantaneous optimizers corresponding to different enstrophy levels $\mathcal{E}_0$ taken as the initial data, i.e., $\phi(x) = \tilde{u}(x; \mathcal{E}_0)$, leads to the following scaling of the maximum enstrophy as a function of the initial enstrophy $\mathcal{E}_0$ (see also Figure 1)

$$\max_{t\in[0,T]} \mathcal{E}(t) \approx C_\alpha \, \mathcal{E}_0^\alpha, \tag{14}$$

where $C_\alpha = 2.681$ and $\alpha = 1.048 \pm 0.018$. Details regarding the calculation of the power–law fits and the discussion of the numerical technique used to solve system (6) are deferred to Section 4.

We note that, as regards the behavior in time of the enstrophy $\mathcal{E}(t)$ characterizing the solutions of initial–value problem (6), two distinct scenarios are possible depending on the values of $\mathcal{E}_0$ and ν: the enstrophy may either decrease monotonously with time, or it may exhibit transient growth followed by eventual decrease. In all cases shown in Figure 1 we made sure to take the length T of the time window sufficiently long, so that the enstrophy maximum always falls inside the interval $[0, T]$. By comparing the exponents in estimate (5) and power–law fit (14), i.e., 3 vs. 1, we conclude that the system evolution starting from the instantaneously optimal state $\tilde{u}$ as the initial condition is in fact quite far from saturating estimate (5). This observation leads to the question whether there may exist initial data which does not solve instantaneous problem (8), but may come closer to saturating (5) than (14). Therefore, one would wish to study the following problem corresponding to the enstrophy growth over a finite time window $[0, T]$

$$\begin{aligned} &\max_{\phi\in H^1(\Omega)} \left\{ \max_{t>0} [\mathcal{E}(t) - \mathcal{E}_0] \right\} \\ &\text{subject to } \begin{cases} \text{System (6)} \\ \mathcal{E}(0) = \mathcal{E}_0 \end{cases}, \end{aligned} \tag{15}$$

where the initial enstrophy value $\mathcal{E}_0$ is a parameter. Due to non–differentiability of the function $\max_t(\cdot)$, problem (15) is in fact non–smooth, and while non–smooth optimization techniques exist [22], in practice such problem remain quite difficult to solve computationally. Thus, we will replace problem (15) with the following computationally more tractable problem

$$\begin{aligned} &\max_{\phi\in H^1(\Omega)} [\mathcal{E}(T) - \mathcal{E}(0)] \\ &\text{subject to } \begin{cases} \text{System (6)} \\ \mathcal{E}(0) = \mathcal{E}_0 \end{cases}, \end{aligned} \tag{16}$$

where the length T of the time window and the initial enstrophy $\mathcal{E}_0$ are two parameters. We note that instead of applying the function $\max_t(\cdot)$ as in (15), in (16) we now perform

a parametric study with respect to the length of the time window. By solving problem (16) for a broad range of values of T and $\mathcal{E}_0$ we will seek to obtain the following power law, cf. (5),

$$\max_{t>0} \tilde{\mathcal{E}}(t) = C_\alpha \mathcal{E}_0^\alpha \tag{17}$$

for some $C_\alpha > 0$ and $0 < \alpha \leq 3$, **where**

$$\tilde{\mathcal{E}}(t) \triangleq \max_{\phi \in H^1(\Omega)} \mathcal{E}(t;\phi) \tag{18}$$

is the enstrophy corresponding to solutions of (6) **with the optimal initial condition** $\tilde{\phi}$ **obtained from** (16). In Section 4 we will present *a posteriori* evidence that no maximizers are in fact lost when problem (16) is solved instead of (15). A numerical approach to solution of problem (16) is introduced in the next Section.

3 Solution of the Finite–Time Optimization Problem

In order to put problem (16) into a suitable form we define the cost functional $\mathcal{J} : H^1(\Omega) \to \mathbb{R}$ as

$$\mathcal{J}(\phi) \triangleq \int_0^T \frac{d\mathcal{E}}{d\tau}\, d\tau = \mathcal{E}(T) - \mathcal{E}_0, \tag{19}$$

where ϕ, the initial data in Burgers system (6), is the control variable, and the right–hand side (RHS) in (19) depends on ϕ through (6) and (7). Optimization problem (16) is now restated as

$$\begin{aligned} &\max_{\phi \in H^1(\Omega)} \mathcal{J}(\phi) \\ &\text{subject to } \frac{1}{2}\left\| \frac{d\phi}{dx} \right\|_{L_2}^2 = \mathcal{E}_0. \end{aligned} \tag{20}$$

We formulate our approach below in the "optimize–then–discretize" framework [23] where the optimality conditions for problem (20) and expressions for the cost functional gradient are derived in the continuous (PDE) setting and only then discretized. Defining the augmented cost functional as

$$\mathcal{J}_\lambda(\phi) \triangleq \mathcal{J}(\phi) + \lambda \left(\frac{1}{2}\left\| \frac{d\phi}{dx} \right\|_{L_2}^2 - \mathcal{E}_0 \right), \tag{21}$$

where $\lambda \in \mathbb{R}$ is the Lagrange multiplier, the first–order optimality condition (with respect to the initial data ϕ) characterizing the maximizer $\tilde{\phi}$ is

$$\forall \phi' \in H^1(\Omega) \qquad \mathcal{J}'_\lambda(\tilde{\phi};\phi') = \mathcal{J}'(\tilde{\phi};\phi') + \lambda \int_0^1 \frac{d\tilde{\phi}}{dx}\frac{d\phi'}{dx}\, dx, \tag{22}$$

where the Gâteaux differential is defined as $\mathcal{J}'(\phi;\phi') \triangleq \frac{d}{d\epsilon}\mathcal{J}(\phi+\epsilon\phi')\big|_{\epsilon=0}$ and ϕ' is an arbitrary perturbation direction. The maximizer $\tilde{\phi}$ is approximated as $\tilde{\phi} = \lim_{n\to\infty}\phi^{(n)}$ using an iterative ascent algorithm based on the Polak–Ribière version of the conjugate gradients method [24] combined with a projection approach ensuring that the constraint in (20) is satisfied (up to numerical round–off errors) at every iteration n. Denoting $p^{(n)}$ the ascent direction at the n–th iteration, we define the function $\psi : \mathbb{R}^+ \to \mathcal{S}_{\mathcal{E}_0}$, where $\mathcal{S}_{\mathcal{E}_0} \triangleq \{\phi \in H^1(\Omega) : \frac{1}{2}\|d\phi/dx\|_{L_2}^2 = \mathcal{E}_0\}$ is the constraint manifold, as

$$\psi(\tau) \triangleq \frac{(2\mathcal{E}_0)^{1/2}}{\left\|\frac{d\phi^{(n)}}{dx} + \tau\frac{dp^{(n)}}{dx}\right\|_{L_2}}(\phi^{(n)} + \tau p^{(n)}) \tag{23}$$

which represent a "radial" projection of the element $(\phi^{(n)} + \tau p^{(n)})$ on the constraint manifold $\mathcal{S}_{\mathcal{E}_0}$. Then, consecutive approximations of the maximizer $\tilde{\phi}$ are computed as follows

$$\phi^{(n+1)} = \psi(\tau_n), \quad n = 1, 2, \dots \tag{24a}$$

$$\phi^{(0)} = \phi_0, \tag{24b}$$

where ϕ_0 is a suitably chosen initial guess, and the optimal step length τ_n is determined via

$$\tau_n = \arg\max_{\tau>0}\left[\mathcal{J}(\psi(\tau))\right], \tag{25}$$

which can be described as "arc minimization" (in contrast to line minimization [24], because the mapping $\tau \to \phi(\tau)$ traces an "arc" on the constraint manifold $\mathcal{S}_{\mathcal{E}_0}$, see Figure 2). Procedure (25) is implemented using an adaptation of Brent's method [28]. Using the Polak–Ribière version of the conjugate gradients method, the ascent direction at the n–th iteration is computed as follows

$$p^{(n)} = \boldsymbol{\nabla}^{H^1}\mathcal{J}^{(n)} - \beta_n p^{(n-1)}, \quad \text{where} \tag{26a}$$

$$\beta_n = \frac{\left\langle \boldsymbol{\nabla}^{H^1}\mathcal{J}^{(n)}, \boldsymbol{\nabla}^{H^1}\mathcal{J}^{(n)} - \boldsymbol{\nabla}^{H^1}\mathcal{J}^{(n-1)}\right\rangle_{H^1}}{\left\|\boldsymbol{\nabla}^{H^1}\mathcal{J}^{(n-1)}\right\|_{H^1}^2}, \tag{26b}$$

where $\langle\cdot,\cdot\rangle$ denotes the inner product in the space indicated by the subscript. A central element of approach based on (23)–(26) is the cost functional gradient $\boldsymbol{\nabla}^{H^1}\mathcal{J}$ representing the infinite–dimensional sensitivity of functional (19) to perturbations $\phi' \in H^1(\Omega)$. It is related to Gâteaux differential via the Riesz Representation Theorem [25] as $\mathcal{J}'(\phi;\phi') = \langle\boldsymbol{\nabla}^{H^1}\mathcal{J}, \phi'\rangle_{H^1(\Omega)}$. As shown in Appendix B, the gradient $\boldsymbol{\nabla}^{H^1}\mathcal{J}$ can be obtained by solving the following boundary–value problem

$$\boldsymbol{\nabla}^{H^1}\mathcal{J} - \ell^2\frac{d}{dx^2}\boldsymbol{\nabla}^{H^1}\mathcal{J} = u^*\big|_{t=0} + \frac{d^2}{dx^2}\phi \quad \text{in } \Omega, \tag{27a}$$

$$\text{Periodic BC}, \tag{27b}$$

where $u^*(t,x)$ is a solution of the *adjoint* system

$$\frac{\partial u^*}{\partial t} + u\frac{\partial u^*}{\partial x} + \nu\frac{\partial^2 u^*}{\partial x^2} = 0 \qquad \text{in } [0,T)\times\Omega, \tag{28a}$$

$$u^*(T,x) = -\frac{d^2}{dx^2}u(T,x) \qquad \text{in } \Omega, \tag{28b}$$

$$\text{Periodic BC} \qquad \text{for } 0 < t \leq T, \tag{28c}$$

and ℓ is a fixed length–scale parameter. It should be noted that u in (28a) and (28b) is the solution of governing system (6) for the given initial data ϕ. We emphasize that by obtaining $\boldsymbol{\nabla}^{H^1}\mathcal{J}$ as solution of problem (27) it is ensured that the cost functional gradient is an element of the Sobolev space $H^1(\Omega)$, rather than only $L_2(\Omega)$. We also remark that the parameter ℓ controls the degree of smoothness of the gradient $\boldsymbol{\nabla}^{H^1}\mathcal{J}$ [26]. A summary of our maximization algorithm is presented below

Algorithm 1 *For given values of T and $\mathcal{E}_0$:*

1. *Set $n = 0$, define tolerance* `tol`.
2. *Set initial guess for control variable ϕ_0.*
3. *Do*
   - *Solve direct problem* (6).
   - *Solve adjoint problem* (28).
   - *Calculate the H^1 gradient with* (27).
   - *Calculate ascent direction $p^{(n)}$ using Polak–Ribière formula* (26).
   - *Find step size τ_n via arc maximization* (25).
   - *Set $\phi^{(n+1)} = \psi(\tau_n)$.*
   - *Evaluate $\Delta\mathcal{J} = \left[\mathcal{J}(\phi^{(n+1)}) - \mathcal{J}(\phi^{(n)})\right]/\mathcal{J}(\phi^{(n)})$.*
   - *$n \mapsto n+1$.*
4. *while $\Delta\mathcal{J} >$ tol.*

Some details concerning the numerical solution of the different PDEs involved in Algorithm 1 will be presented in Section 4.

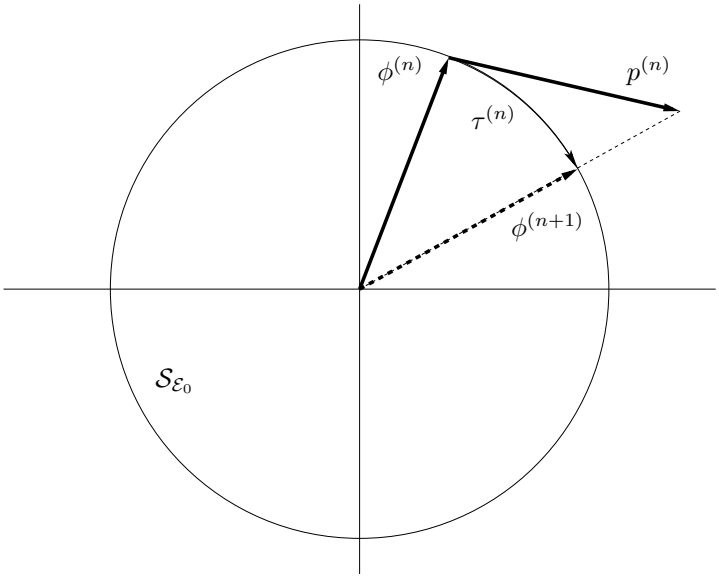

Figure 2: Schematic representation of arc maximization defined in (23)–(25). The dotted line represents the direction of the projection.

4 Results

In this Section we report the computational results obtained applying Algorithm 1 to solve problem (20) for a broad range of time windows T and initial enstrophies $\mathcal{E}_0$, namely $T \in [10^{-3}, 1]$ and $\mathcal{E}_0 \in [10^{-3}, 10^3]$. In all computations reported hereafter we will assume $\nu = 10^{-3}$. Direct and adjoint system, (6) and (28), were solved with the pseudo–spectral Fourier–Galerkin method with dealiasing where the equations were discretized using $N = 1024$ grid points. Discretization in time combined the Crank–Nicolson method applied to the viscous terms with the RK4 method applied to the advection terms. The time step was adjusted individually based on the CFL condition in every case. The tolerance used in Algorithm 1 was $\texttt{tol} = 10^{-12}$. All elements of Algorithm 1 were thoroughly validated and **the convergence of the optimization results with refinement of the spatial resolution was carefully verified on a number of selected cases**. We refer the reader to dissertation [29] for all details. **Exponents of the power laws reported in this work are given in the form**

$$e = e_0 \pm \sigma_e,$$

where e_0 is the exponent obtained by a global least–squares fit performed over the entire scaling region, and

$$\sigma_e = \sqrt{\frac{1}{M-1}\sum_{i=1}^{M}(e_i - e_0)^2}$$

is the "standard deviation" in which e_i, $i = 1, \ldots, M$, are the exponents obtained by "local" least–squares fits based on three adjacent data points.

Given the nonlinearity of Burgers equation (6a), optimization problem (20) will in general be non–convex, hence optimality condition (22) characterizes only *local* maximizers. Consequently, depending on the choice of the initial guess ϕ_0, Algorithm 1 may converge to different locally maximizing solutions. While there are no general methods allowing one to identify global maximizers in such problems, it is very important to carry out a systematic search for such solutions. We did this for every value of T and $\mathcal{E}_0$ using a family of initial guesses of the form

$$\phi_0(x) = -\frac{\sqrt{\mathcal{E}_0}}{\pi m}\sin(2\pi m x), \qquad m = 1, 2, \ldots, \tag{29}$$

where m is the wavenumber (we have also tested several initial guesses given in terms of functions other than trigonometric, e.g., instantaneously optimal solutions $\tilde{u}$, cf. (10), but in all cases the same maximizers were found as using (29) for the given value of m). The rationale for using initial guesses (29) is that for different wavenumbers m such functions are orthogonal to each other in the space $H^1(\Omega)$, hence initializing Algorithm 1 in such orthogonal directions represents an efficient way to "probe" an infinite–dimensional control space. The optimal initial conditions $\tilde{\phi}_{(m)}$ found using initial guesses (29) with $m = 1, 2, 3, 4$ and corresponding to different values of T and $\mathcal{E}_0$ are shown in Figure 3. While the optimal initial conditions found for different wavenumbers in (29) are clearly different, they exhibit similar trends with changes of the parameters. In particular, we note that for a fixed $\mathcal{E}_0$ and increasing T the fields $\tilde{\phi}_{(m)}$, $m = 1, \ldots, 4$ change from a shock wave type solution to rarefaction wave type solutions.

In order to establish correspondence between optimizing solutions obtained from initial guesses (29) with different wavenumbers m, we consider the following rescaling of Burgers equation (6). Given two domains $\Omega = [0, 1]$ and $\Omega_L = [0, 1/L]$, where $L \in \mathbb{N}$, and the corresponding independent variables $x \in \Omega$ and $\xi \in \Omega_L$, we have the relations

$$\xi \triangleq \frac{x}{L}, \quad \tau \triangleq \frac{t}{L^2}, \tag{30a}$$

$$w(\tau, \xi) \triangleq L\, u(t(\tau), x(\xi)), \tag{30b}$$

and the following transformations for the derivatives

$$\frac{\partial w}{\partial \tau} = L^3 \frac{\partial u}{\partial t}, \qquad \frac{\partial w}{\partial \xi} = L^2 \frac{\partial u}{\partial x}, \qquad \frac{\partial^2 w}{\partial \xi^2} = L^3 \frac{\partial^2 u}{\partial x^2}. \tag{31}$$

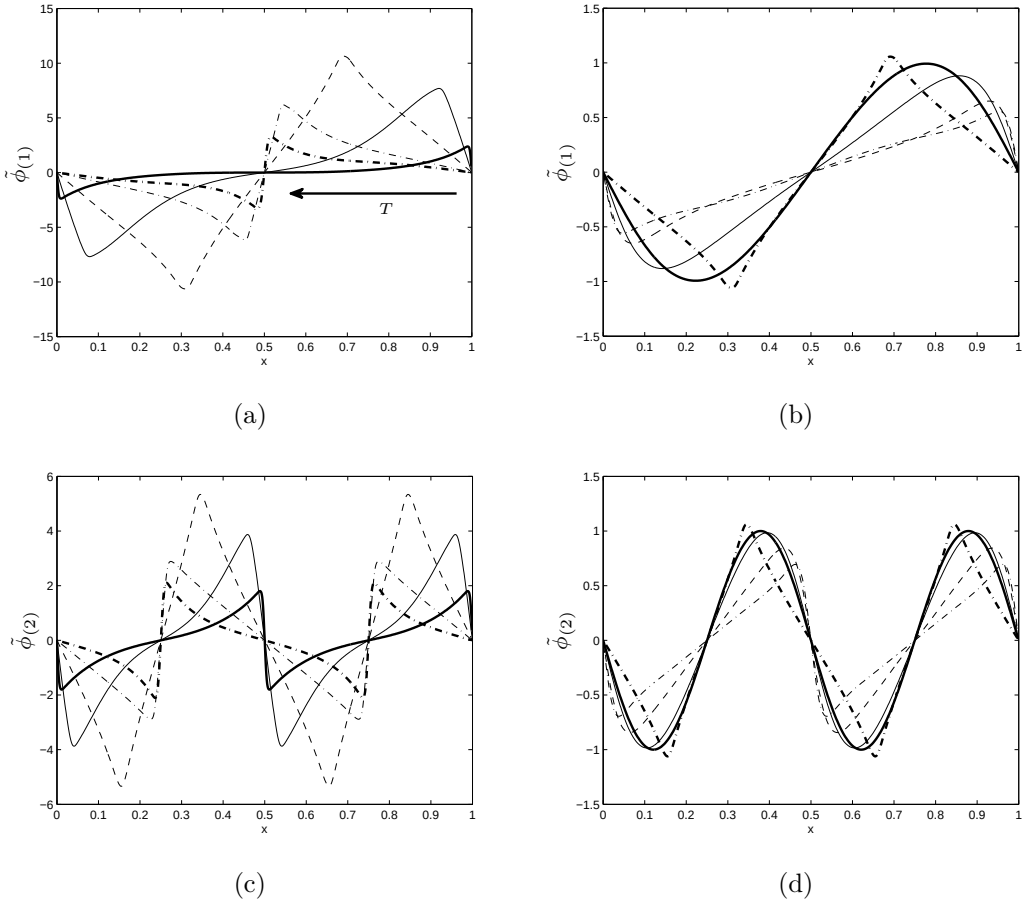

Figure 3: Optimal initial conditions (a,b) $\tilde{\phi}_{(1)}$ and (c,d) $\tilde{\phi}_{(2)}$. Figures (a,c) correspond to fixed enstrophy $\mathcal{E}_0 = 10^3$ and different time intervals: (thick solid line) $T = 10^{-3}$, (thin solid line) $T = 10^{-2}$, (thin dashed line) $T = 10^{-1.5}$, (thin dotted line) $T = 10^{-1}$ and (thick dotted line) $T = 10^0$; the arrow in Figure (a) indicates the trend with increasing T. Figures (b,d) correspond to a fixed time interval $T = 10^{-1.5}$ and different enstrophies: (thin solid line) $\mathcal{E}_0 = 10^{-3}$, (thin dashed line) $\mathcal{E}_0 = 10^{-1.5}$, (thick solid line) $\mathcal{E}_0 = 10^0$, (thick dashed line) $\mathcal{E}_0 = 10^{1.5}$ and (thick dotted line) $\mathcal{E}_0 = 10^3$.

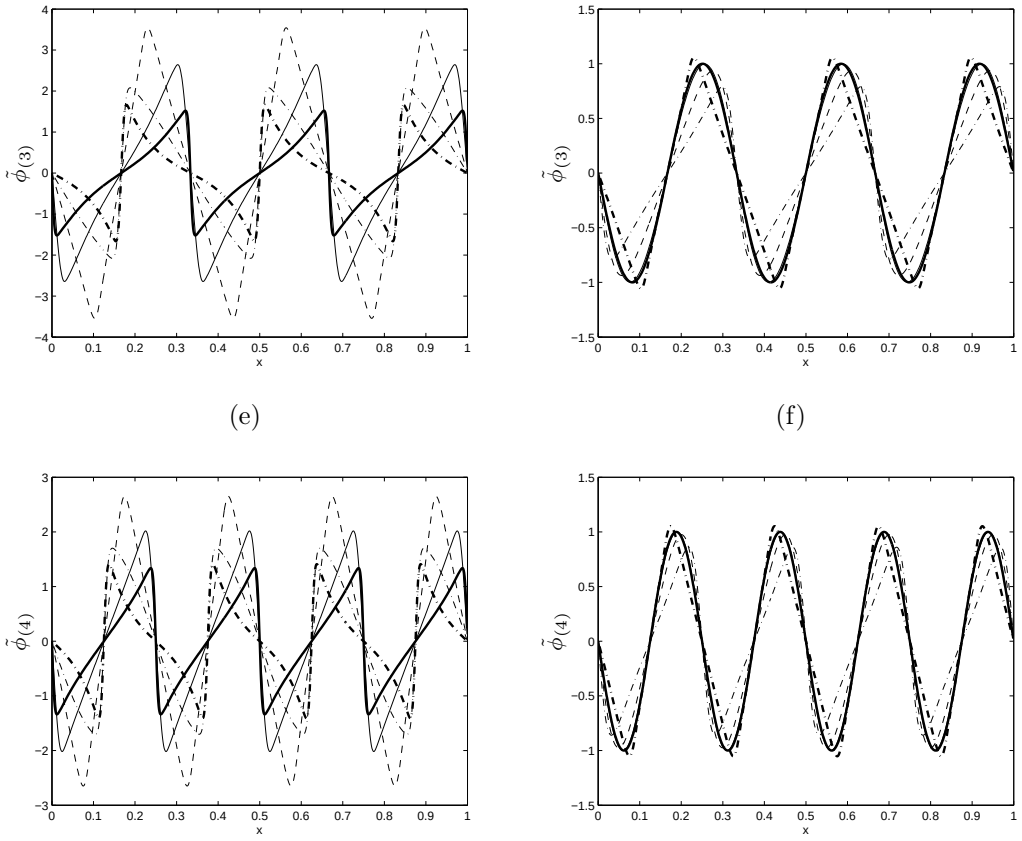

Figure 3: (continued) Optimal initial conditions (e,f) $\tilde{\phi}_{(3)}$ and (g,h) $\tilde{\phi}_{(4)}$. See previous caption for details.

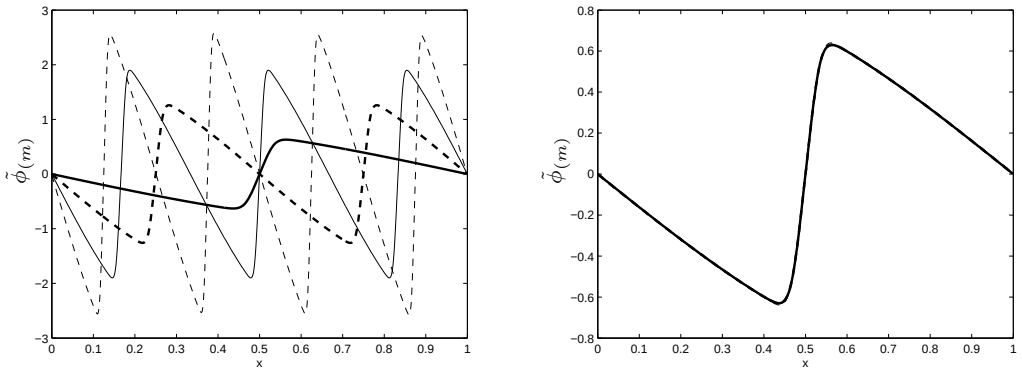

(a) (b)

Figure 4: (a) Optimal initial conditions $\tilde{\phi}_{(m)}$ obtained with initial guesses (29) with wavenumbers (thick solid) $m = 1$, (thick dashed) $m = 2$, (thin solid) $m = 3$ and (thin dashed) $m = 4$; (b) the same optimal initial conditions as in Figure (a) rescaled according to (30).

If u is a solution of Burgers equation (6) in $(0, T) \times \Omega$, then

$$0 = \partial_t u + u\partial_x u - \nu\partial_x^2 u = \frac{1}{L^3}\left(\partial_\tau w + w\partial_\xi w - \nu\partial_\xi^2 w\right) \tag{32}$$

which means that w defined in (30b) is also solution of Burgers equation in $(0, T/L^2)\times\Omega_L$. We note that changing the wavenumber of initial guess (29) from 1 to some $m > 1$ can in fact be interpreted as rescaling (30) with $L = m$, provided the solution enstrophy is also rescaled according to

$$\mathcal{E}_L(\tau) = L^4\mathcal{E}\left(\tfrac{t}{L^2}\right). \tag{33}$$

Therefore, by adjusting the length of the time window and the enstrophy level as in (30a) and (33), optimization problems (20) solved with initial guesses (29) characterized by different wavenumbers m are shown to be equivalent. Indeed, in Figure 4a we present the optimal initial conditions $\tilde{\phi}_{(m)}$ obtained starting from initial guesses (29) with $m = 1, 2, 3, 4$, where the parameters $\mathcal{E}_0$ and T were in all cases determined from (30a) and (33). In Figure 4b we note that when rescaling (30) is applied to these different maximizers $\tilde{\phi}_{(m)}$, they all collapse, implying that the maximizers $\tilde{\phi}_{(m)}$ corresponding to initial guesses with different $m > 1$ are in fact rescaled copies of one "fundamental" maximizer $\tilde{\phi}_{(1)}$.

In an effort to find local maximizers $\tilde{\phi}$ characterized by the largest enstrophy growth, we also solved problem (20) with initial guesses formed as linear combinations of expressions (29) with different values of the wavenumber m. In all such attempts, however, the maximizers found would always be the same as the ones obtained for the initial

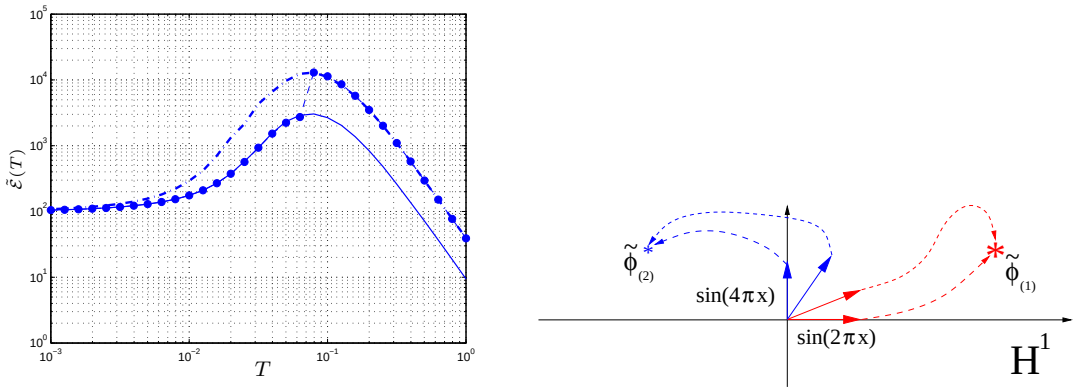

(a) (b)

Figure 5: (a) Terminal enstrophy $\tilde{\mathcal{E}}(T)$ vs. length T of the optimization window corresponding to the initial guesses (circles) $\phi_0(x) = A_1 \sin(2\pi x) + A_2 \sin(4\pi x)$, where A_1 and A_2 are chosen so that $\mathcal{E}_0 = 10^2$, (dashed line) (29) with $m = 1$ and (solid line) (29) with $m = 2$; (b) schematic illustrating convergence to the fundamental maximizer $\tilde{\phi}_{(1)}$ and its rescaled copy $\tilde{\phi}_{(2)}$ starting from different initial guesses represented by arrows at the origin.

guesses with one wavenumber only. Typical outcomes from such calculations are presented in Figure 5 where we show the results of optimizations starting from initial guess $\phi_0(x) = A_1 \sin(2\pi x) + A_2 \sin(4\pi x)$, where A_1 and A_2 are chosen so that $\frac{1}{2}\int_0^1 |d\phi_0/dx|^2\, dx = \mathcal{E}_0$. We see that this approach produces the same results as when initial guess (29) is used with $m = 1$ or $m = 2$. This situation is schematically illustrated in Figure 5b, where the big and small star represent the maximizer $\tilde{\phi}_{(1)}$ and its rescaled copy $\tilde{\phi}_{(m)}$ corresponding to $m = L = 2$, and the vectors at the origin represent the different initial guesses used to find these solutions. We also used initial guesses generated randomly according to several different rules, and in those attempts as well the maximum enstrophy found was not greater than when (29) is used. Thus, in view of this analysis, we conclude that in determination of the exponent in power law (17) we can, without loss of generality, use the results obtained using (29) with $m = 1$ as the initial guess, and this is the data that will be discussed below (for simplicity, we will drop the subscripts m).

In Figures 6a and 6b we show, respectively, the terminal enstrophy $\tilde{\mathcal{E}}(T)$ and the maximum enstrophy $\max_{t\in[0,T]} \tilde{\mathcal{E}}(t)$ as functions of the length T of the time window and for different values of the initial enstrophy $\mathcal{E}_0$. We note that these data in fact coincide for a large part of the parameter values meaning that in those cases the enstrophy maximum is attained at the end of the time window, i.e., $\max_{t\in[0,T]} \tilde{\mathcal{E}}(t) = \tilde{\mathcal{E}}(T)$. In some cases the

enstrophy maximum is actually attained *inside* the interval $[0,T]$ (e.g., for $\mathcal{E}_0 \gtrsim 10^3$ and $T \gtrsim 2\cdot 10^{-2}$). Plotting this data as a function of $\mathcal{E}_0$ with T acting as a parameter shows that the relations $\max_{t\in[0,T]} \tilde{\mathcal{E}}(t)$ vs. $\mathcal{E}_0$ and $\tilde{\mathcal{E}}(T)$ vs. $\mathcal{E}_0$ have in fact the same envelope, that is,

$$\forall\, \mathcal{E}_0 > 0, \quad \mathcal{E}_{\max} \triangleq \max_T \tilde{\mathcal{E}}(T) = \max_T \left[\max_{t\in[0,T]} \tilde{\mathcal{E}}(t) \right]. \tag{34}$$

This observation may suggest that by solving optimization problem (16) instead of the more fundamental problem (15) we do not in fact miss any maximizers. In Figure 7 we note that, as predicted by analytic bound (5), there are two regimes characterized by distinct power laws of the form

$$\mathcal{E}_{\max} = \begin{cases} C_{\alpha_1}\, \mathcal{E}_0^{\alpha_1}, & \mathcal{E}_0 \to 0 \\ C_{\alpha_2}\, \mathcal{E}_0^{\alpha_2}, & \mathcal{E}_0 \to \infty \end{cases} \tag{35}$$

with $\alpha_1 = 1.000 \pm 0.003$ and $\alpha_2 = 1.531 \pm 0.022$, showing that, while for small $\mathcal{E}_0$ the exponent in (17) is close to one and hence in agreement with (5), for large $\mathcal{E}_0$ the exponent in the power law is approximately $3/2$ which is significantly less than the value of 3 predicted by (5).

There are also other power laws one can uncover in our data. For example, in Figure 8 we show the dependence of

$$T_{\max} \triangleq \arg\max_T [\max_{t\in[0,T]} \tilde{\mathcal{E}}(t)], \tag{36}$$

which represents the length of the time window yielding the largest enstrophy growth for a given $\mathcal{E}_0$, as a function of $\mathcal{E}_0$. A power–law behavior can be observed for this quantity for $\mathcal{E}_0$ sufficiently large and is given by

$$T_{max} \approx C_\eta\, \mathcal{E}_0^\eta, \qquad \text{as } \mathcal{E}_0 \to \infty, \tag{37}$$

where $C_\eta = 0.7619$ and $\eta = -0.497 \pm 0.017$. It is interesting to analyze the relation between the kinetic energy $\mathcal{K}_0 \triangleq \frac{1}{2}\int_0^1 u(0,x)^2\, dx$ and the enstrophy $\mathcal{E}_0$ for the instantaneous and finite–time optimizers $\tilde{u}$ and $\tilde{\phi}$. This data is shown in Figure 9 where power–laws of the form

$$\mathcal{K}_0 \approx C_\theta\, \mathcal{E}_0^\theta, \qquad \text{as } \mathcal{E}_0 \to \infty, \tag{38}$$

are clearly observed in both cases. The exponents obtained are $\theta = 0.678 \pm 0.005$ for the instantaneous case and $\theta = 0.978 \pm 0.017$ for the finite–time case. The proximity of the latter exponent to unity implies that the optimizers $\tilde{\phi}$ are close to saturating Poincaré's inequality. The constant $C_\theta = 0.0238$ in (38) corresponds to about 97% of the Poincaré constant $C_P = 1/(2\pi)$ (as is well known, see e.g., [10], the trigonometric functions sin and cos are the only periodic functions exactly saturating Poincaré's inequality, so we should not expect C_θ to be equal to C_P^2).

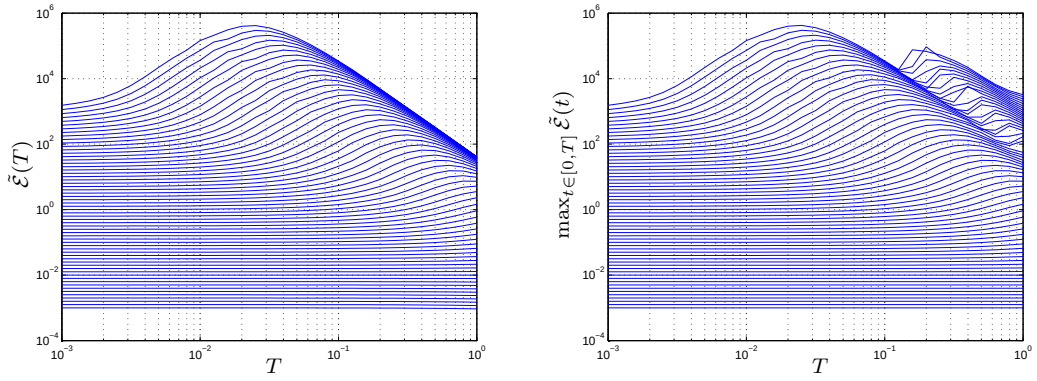

(a) (b)

Figure 6: (a) Final enstrophy $\tilde{\mathcal{E}}(T)$ and (b) maximum enstrophy $\max_{t\in[0,T]} \tilde{\mathcal{E}}(t)$ as functions of the length T of the time window for different initial enstrophies $\mathcal{E}_0$.

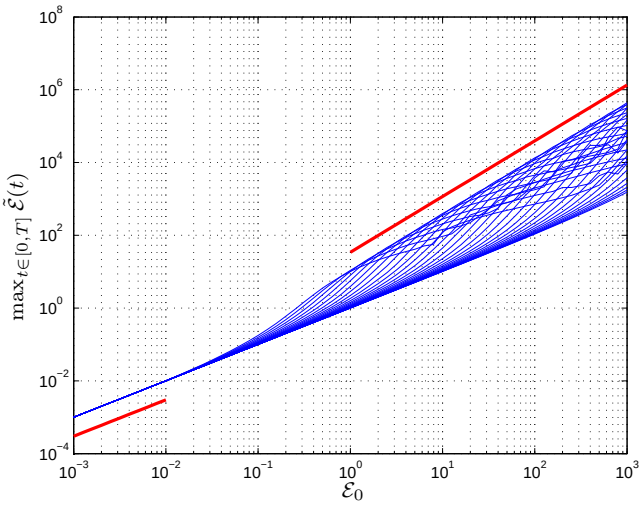

(a)

Figure 7: Maximum enstrophy $\max_{t\in[0,T]} \tilde{\mathcal{E}}(t)$ as a function of initial enstrophy $\mathcal{E}_0$ for different T. **Two distinct power laws can be observed characterized by the exponents $\alpha_1 \approx 1$ for small $\mathcal{E}_0$, and $\alpha_2 \approx 3/2$ for large $\mathcal{E}_0$, cf.** (35)**.**

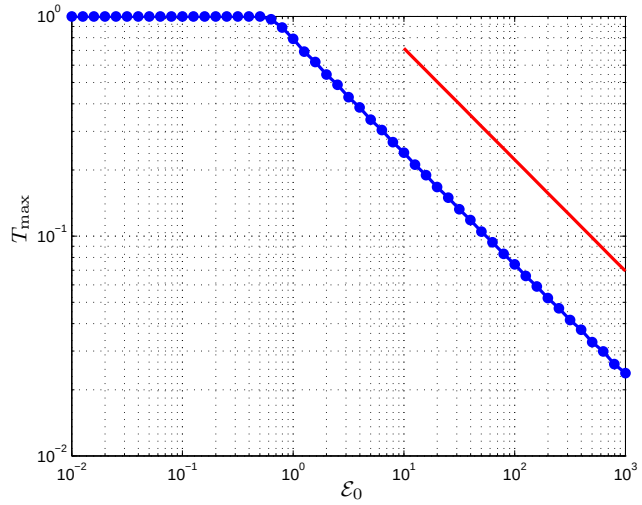

(a)

Figure 8: Maximization time $T_{\max}$ as a function of initial enstrophy $\mathcal{E}_0$. The exponent of the corresponding power law is found to be $\eta \approx -1/2$, cf. (37).

We close this Section by offering an alternative view of the obtained results, namely, from the perspective of the complex–plane singularities associated with different solutions (cf. discussion in Introduction). The key quantity of interest is the (time–dependent) width $\delta(t)$ of the analyticity strip representing the time evolution of the distance from the real line to the nearest singularity $z_0(t)$ in the complex plane, i.e., $\delta(t) \triangleq \Im\{z_0(t)\}$. It is approximated using the method developed in [16] based on an asymptotic expansion of the Fourier spectrum of the solution $u(t,\cdot)$. The time evolution of $\delta(t)$ for solutions of the instantaneous and finite–time (with two different T) optimization problems in shown in Figure 10a, whereas the corresponding time–evolution of the enstrophy $\mathcal{E}(t)$ is shown in Figure 10b. We note that in all cases the minima of $\delta(t)$ correspond to the maxima of $\mathcal{E}(t)$ with the analyticity strip achieving smaller widths in the cases where the finite–time optimizers $\tilde{\phi}$ were used as the initial data. This confirms that the corresponding solutions of Burgers problem (6) can be indeed regarded as "less regular" than the solutions starting from the instantaneously optimal initial condition $\tilde{u}$.

5 Discussion and Conclusions

In this work we have developed a computational approach allowing one to identify solutions of an initial–value problem for a PDE which may saturate analytic bounds for

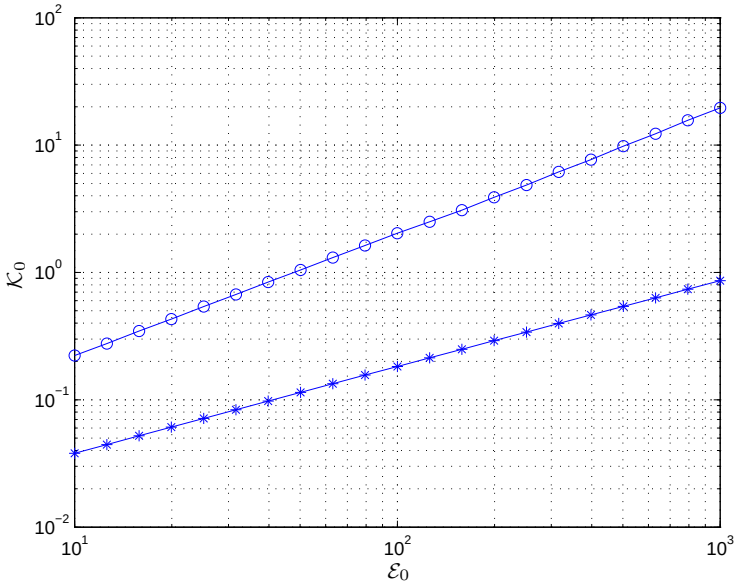

Figure 9: Energy $\mathcal{K}_0$ of the initial condition as a function of its enstrophy $\mathcal{E}_0$ for (stars) solutions $\tilde{u}$ of instantaneous optimization problem (8) and (circles) solutions $\tilde{\phi}$ of the finite–time optimization problem (16).

the growth of certain norms of the solution. This approach is formulated as a PDE–constrained optimization problem which is solved numerically with a gradient–based ascent method. The proposed method can therefore provide insights as to whether or not a given norm estimate is sharp. Motivated by the 3D regularity problem for the Navier–Stokes system, we have applied this method to study the estimates for the maximum enstrophy growth in 1D Burgers equation and concluded that the best available estimates do not appear sharp. While the proposed method can in principle only characterize local maximizers, we have shown computational evidence that the optimization problem may admit a countably-infinite family of maximizers parametrized by the dominating wavenumber such that each maximizer in the family is a rescaled copy of one fundamental maximizer. The time–dependent solutions corresponding to such optimal initial data reveal a number of power laws, and the corresponding exponents are collected in Table 1 together with analytic predictions and the results corresponding to the instantaneously optimal initial data computed in [10].

We speculate that, if a certain norm bound is found not to be sharp, the proposed approach might provide some guidance how the bound could be tightened up. In this regard, we note that in the derivation of estimate (5) in Appendix A an intermediate inequality (45) was used to obtain an upper bound for $\int_0^t \mathcal{E}(s)ds$. If we use the exact

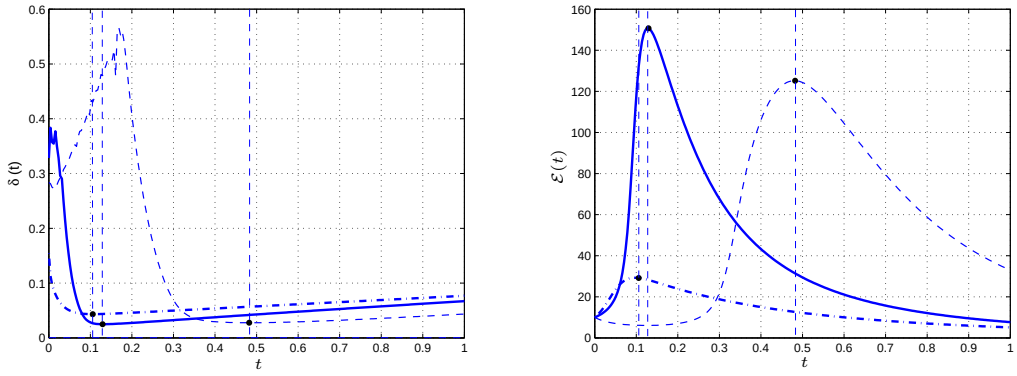

(a) (b)

Figure 10: (a) Time evolution of the width $\delta(t)$ of analyticity strip for solutions to Burgers system (6) with initial condition (thick, dashed line) $\tilde{u}$ obtained from instantaneous optimization problem (8), (thin, dashed line) $\tilde{\phi}$ obtained form finite–time optimization problem (16) with $T = 0.1$ and (thick line) $\tilde{\phi}$ obtained form finite–time optimization problem (16) with $T = 1$; (b) time evolution of enstrophy $\mathcal{E}(t)$ for the same solutions as in Figure (a); the vertical lines represent the times when the minima and maxima of the two quantities are attained.

power law	analytic estimate	Instantaneous optimization problem (8)	Finite–time optimization problem (16)
$\max_{t\in[0,T]} \tilde{\mathcal{E}}(t) \approx C_\alpha \mathcal{E}_0^\alpha$	$\alpha = 3$	$\alpha = 1.048 \pm 0.018$	$\alpha = 1.531 \pm 0.022$
$T_{max} \approx C_\eta \, \mathcal{E}_0^\eta$	—	$\eta = -0.607 \pm 0.02$	$\eta = -0.497 \pm 0.017$
$\mathcal{K}_0 \approx C_\theta \, \mathcal{E}_0^\theta$	$\theta = 1$	$\theta = 0.678 \pm 0.005$	$\theta = 0.978 \pm 0.017$
$\mathcal{K}(T_{\max}) \approx C_\mu \, \mathcal{E}_0^\mu$	—	$\mu = 0.695 \pm 0.001$	$\mu = 1.008 \pm 0.013$
$\mathcal{K}_0 - \mathcal{K}(T_{\max}) \approx C_\gamma \, \mathcal{E}_0^\gamma$	—	$\gamma = 0.44 \pm 0.032$	$\gamma = 0.68 \pm 0.25$

Table 1: Summary of the exponents characterizing the power laws obtained via analytic estimates and from the solution of the instantaneous and finite–time optimization problems **in the limit of large** $\mathcal{E}_0$.

value of this integral instead, cf. equation (44), we would arrive at

$$\mathcal{E}^{1/3}(t) - \mathcal{E}_0^{1/3} \leq \frac{C_1}{3} \int_0^t \mathcal{E}(s) ds = \frac{C_1}{6\nu} [\mathcal{K}_0 - \mathcal{K}(t)]. \tag{39}$$

The main difference between this last inequality and estimate (5) is that we do not know, *a priori*, how the difference between the initial and terminal energy scales with the initial enstrophy. More specifically, if we knew that this difference follows a power law

$$\mathcal{K}_0 - \mathcal{K}(t) \approx C_\gamma \, \mathcal{E}_0^\gamma \tag{40}$$

for some $0 < \gamma \leq 1$, then it might be possible to obtain a sharper estimate in inequality (48) depending on the value of γ **(note that, as shown in Appendix A, $\gamma = 1$ in estimate** (5)**).** Figure 11 shows the difference $\mathcal{K}_0 - \mathcal{K}(T_{\max})$, with $T_{\max}$ defined in (36), as a function of the initial enstrophy $\mathcal{E}_0$. Using the least–squares fitting described in Section 4, we find that $\gamma = 0.68 \pm 0.25$ in (40) which may give a more accurate *a posteriori* estimate for the difference in energy levels, hence a better approximation for the integral of the enstrophy over the time interval than (45). This may be, in our opinion, one reason why the analytic estimate fails to be sharp and overestimates the enstrophy growth. For comparison, Figure 11 also shows the difference $\mathcal{K}_0 - \mathcal{K}(T_{\max})$ for the case where the instantaneous optimizer $\tilde{u}$ is used as the initial condition and the corresponding exponent of power law (40) is $\gamma = 0.44 \pm 0.032$. We need to emphasize, however, that the analysis presented in this paragraph is not rigorous and the exponents found do not represent the worst cases, but only the scaling observed for particular families of solutions.

We conclude by mentioning some future directions for this research. **Our next step, already underway, is to address analogous questions for the 2D Navier–Stokes system in a periodic domain. Starting from smooth initial data, the 2D Navier–Stokes problem also leads to smooth solutions existing globally in time. The difference with the present case and the 3D case is that the relevant quantity to be maximized is the L_2 norm of the vorticity gradient, the so–called palinstrophy, rather than enstrophy (which cannot grow in 2D flows without forcing). Some estimates concerning the rate of growth of palinstrophy are available in [30]. An ultimate goal of this research effort** is to solve a maximization problem analogous to (16) for the 3D Navier–Stokes system. The principal idea is to observe whether the maximum enstrophy may grow in time at a rate that could lead to a blow–up in finite time, cf. (2). **Formulation of the optimization problem in 2D and in 3D will be essentially the same as discussed in the present study with the cost functional gradient expressed in terms of solutions of a suitably defined adjoint system. Flow optimization problems of this type have already been studied in the literature (although admittedly**

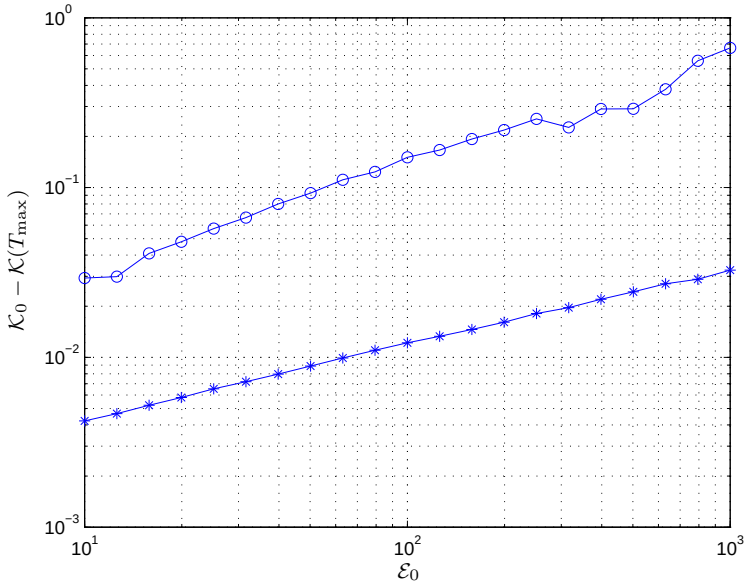

Figure 11: Difference $\mathcal{K}_0 - \mathcal{K}(T_{\max})$, cf. (40), as a function of initial enstrophy $\mathcal{E}_0$ for (stars) instantaneously optimal initial data (10) and (circles) initial data obtained from finite–time optimization problem (20).

for rather low Reynolds numbers in the 3D case) and we refer the reader to the monograph [23] and the papers [31, 32] for some results. While in the 2D case this task appears fairly straightforward due to moderate computational cost and uncomplicated analysis of the results, this will no longer be the case in 3D where the computational cost of solving the optimization problem will be extremely large. As regards the formulation of our approach, an interesting alternative may be to recast the PDE–constrained optimization problem in terms of complex plane singularities (i.e., to directly minimize the width of the analyticity strip).

Acknowledgments

The authors wish to thank C. Doering for his valuable advice, especially as regards derivation of estimate (5) **in Appendix A, and for his constant encouragement of this research.** The authors are also grateful to D. Pelinovsky, D. Viswanath and K. Ohkitani for many helpful discussions. The research was funded by the Ontario Ministry of Research and Innovation through an Early Researcher Award (ERA).

A Finite–Time Bound for Enstrophy Growth

To obtain the finite–time bound for enstrophy from equation (5) we start with the energy $\mathcal{K}$ defined as

$$\mathcal{K}(t) = \frac{1}{2}||u(\cdot,t)||^2_{L_2} = \frac{1}{2}\int_0^L |u(t,x)|^2 dx \tag{41}$$

and its rate of growth

$$\frac{d\mathcal{K}}{dt} = -\nu\int_0^L \left(\frac{\partial u}{\partial x}\right)^2 dx = -\nu\left\|\frac{\partial u}{\partial x}\right\|^2_{L_2}, \tag{42}$$

where for generality we assumed the domain $[0, L]$ (to fix attention, in the main body of this work we set $L = 1$). We notice that the energy is a decreasing function of time bounded by the energy of the initial data, i.e.,

$$\mathcal{K}(t) \leq ||u(\cdot,0)||^2_{L_2} = ||\phi||^2_{L_2}, \qquad \forall t \geq 0. \tag{43}$$

Integrating equation (42) in time we find that

$$\frac{1}{2\nu}\left[\mathcal{K}_0 - \mathcal{K}(t)\right] = \int_0^t \mathcal{E}(s)ds, \quad t > 0, \tag{44}$$

where $\mathcal{K}_0 \triangleq \mathcal{K}(0)$. Since $\mathcal{K}(t) > 0 \; \forall \; t$, we obtain

$$\int_0^t \mathcal{E}(s)ds \leq \frac{1}{2\nu}\mathcal{K}_0. \tag{45}$$

Rewriting the right–hand side of inequality (4) as $C_0\,\mathcal{E}\mathcal{E}^{2/3}$, where $C_0 \triangleq \frac{3}{2}\left(\frac{1}{\pi^2\nu}\right)^{1/3}$, we obtain

$$3\,\frac{d}{dt}\mathcal{E}^{1/3} \leq C_0\mathcal{E} \tag{46}$$

which upon integration in time leads to

$$\mathcal{E}^{1/3}(t) - \mathcal{E}_0^{1/3} \leq \frac{C_0}{3}\int_0^t \mathcal{E}(s)ds \leq \frac{C_0}{6\nu}\mathcal{K}_0 \tag{47a}$$

$$\leq \frac{L^2}{16}\left(\frac{1}{\pi^2\nu}\right)^{4/3}\mathcal{E}_0, \tag{47b}$$

where the fact that the fields u have zero mean allows us to use Poincaré's inequality $\mathcal{K}_0 \leq \left(\frac{L}{2\pi}\right)^2\mathcal{E}_0$ in the last expression. Finally, we obtain

$$\mathcal{E}(t) \leq \left[\mathcal{E}_0^{1/3} + \left(\frac{L}{4}\right)^2\left(\frac{1}{\pi^2\nu}\right)^{4/3}\mathcal{E}_0\right]^3. \tag{48}$$

B Extraction of Cost Functional Gradients

While these calculation are quite standard, they are included here to make the paper self–contained. We begin by calculating the Gâteaux derivative of $\mathcal{J}$

$$\mathcal{J}'(\phi;\phi') = \int_0^1 \frac{\partial u(T,x)}{\partial x}\frac{\partial u'(T,x)}{\partial x}\,dx - \int_0^1 \frac{\partial \phi(x)}{\partial x}\frac{\partial \phi'(x)}{\partial x}\,dx, \tag{49}$$

where $u'(t,x)$ is the solution of the "perturbation" system

$$\frac{\partial u'}{\partial t} + \frac{\partial uu'}{\partial x} - \nu\frac{\partial^2 u'}{\partial x^2} = 0 \qquad \text{in } \Omega\times(0,T], \tag{50a}$$

$$u'(x) = \phi'(x) \qquad \text{in } \Omega \text{ at } t=0, \tag{50b}$$

$$\text{Periodic BC} \qquad \text{for } t>0. \tag{50c}$$

Applying integration by parts to the integrals in (49) and using periodic boundary conditions (50c) we get

$$\mathcal{J}'(\phi;\phi') = -\int_0^1 \frac{\partial^2 u(T,x)}{\partial x^2}u'(T,x)\,dx + \int_0^1 \frac{\partial^2\phi(x)}{\partial x^2}\phi'(x)\,dx. \tag{51}$$

Multiplying equation (50a) by the adjoint variable $u^* : [0,T]\times\Omega\to\mathbb{R}$ and integrating with respect to both space and time yields

$$\begin{aligned} 0 &= \int_0^T\int_0^1 \left(\frac{\partial u'}{\partial t} + \frac{\partial uu'}{\partial x} - \nu\frac{\partial^2 u'}{\partial x^2}\right)u^*\,dx\,dt \\ &= \int_0^1 \left[u^*u'\right]_0^T\,dx - \int_0^T\int_0^1 \left(\frac{\partial u^*}{\partial t} + u\frac{\partial u^*}{\partial x} + \nu\frac{\partial^2 u^*}{\partial x^2}\right)u'\,dx\,dt. \end{aligned}$$

Setting $\frac{\partial u^*}{\partial t} + u\frac{\partial u^*}{\partial x} + \nu\frac{\partial^2 u^*}{\partial x^2} = 0$, cf. (28a), in the last equation above reduces it to

$$\int_0^1 \phi'(x)u^*(0,x)\,dx = \int_0^1 u'(T,x)u^*(T,x)\,dx \tag{52}$$

which, upon setting $u^*(T,x) = -\frac{d^2}{dx^2}u(T,x)$, cf. (28b), and substituting in equation (51), yields

$$\mathcal{J}'(\phi;\phi') = \int_0^1 \left[u^*(0,x) + \frac{d^2}{dx^2}\phi(x)\right]\phi'(x)\,dx = \left\langle \nabla\mathcal{J}, \phi'\right\rangle_{L_2}. \tag{53}$$

In (53) we interpreted the Gâteaux differential in the light of Riesz Representation Theorem [25] as an L_2 inner product which allows us to identify the L_2 gradient of the cost functional as

$$\boldsymbol{\nabla}^{L^2}\mathcal{J} = u^*(x)\big|_{t=0} + \frac{d^2}{dx^2}\phi(x). \tag{54}$$

However, in our maximization approach, cf. (26), we require our cost functional gradients to be from the Sobolev space $H^1(\Omega)$, hence, reinterpreting (53) in terms of the corresponding $H^1(\Omega)$ inner product, we obtain the gradient $\boldsymbol{\nabla}^{H^1}\mathcal{J}$ as a solution of elliptic boundary–value problem (27) in which (54) appears as the right–hand side.

References

[1] Ch. R. Doering, "The 3D Navier–Stokes Problem", *Annual Review of Fluid Mechanics* **41**, 109–128, (2009).

[2] J. Leray, "Sur le mouvement d'un liquide visqueux emplissant l'espace", *Acta Math.* **63**, 193–248, (1934).

[3] C. Fefferman, "Existence and smoothness of the Navier–Stokes equation" *Clay Millennium Prize Problem Description* available at `http://www.claymath.org/millennium/Navier-Stokes_Equations/`, (2000).

[4] P. Constantin and C. Foias C, *Navier-Stokes Equations*, Chicago University Press, (1988).

[5] C. R. Doering and J. D. Gibbon, *Applied Analysis of the Navier–Stokes Equations*, Cambridge University Press, (1995).

[6] R. Temam, *Navier–Stokes Equations: Theory and Numerical Analysis*, North Holland, (1995).:

[7] J. D. Gibbon, M. Bustamante and R. M. Kerr, "The three–dimensional Euler equations: singular or non–singular?", *Nonlinearity* **21**, 123–129, (2008).

[8] K. Ohkitani, "A miscellany of basic issues on incompressible fluid equations", *Nonlinearity* **21**, 255–271, (2008).

[9] C. Foias and R. Temam, "Gevrey class regularity for the solutions of the Navier–Stokes equations", *J. Funct. Anal.* **87**, 359–369, (1989).

[10] L. Lu, *Bounds on the enstrophy growth rate for solutions of the 3D Navier-Stokes equations*, Ph.D. dissertation, The University of Michigan, (2006).

[11] L. Lu and C. R. Doering, "Limits on Enstrophy Growth for Solutions of the Three–dimensional Navier–Stokes Equations" *Indiana University Mathematics Journal* **57**, 2693–2727, (2008).

[12] R. M. Kerr, "Evidence for a singularity of the three–dimensional incompressible Euler equations" *Phys. Fluids A* **5**, 1725–1746, (1993).

[13] T. Y. Hou, "Blow–up or no blow–up? Unified computational and analytic approach to 3D incompressible Euler and Navier–Stokes equations", *Acta Numerica* (2009), 277–346.

[14] R. B. Pelz, "Symmetry and the hydrodynamic blow–up problem", *J. Fluid Mech.* **444**, 299–320, (2001).

[15] K. Ohkitani and P. Constantin, "Numerical study of the Eulerian–Lagrangian analysis of the Navier-Stokes turbulence", *Phys Fluids 20*, 075102-1–11 (2008).

[16] C. Sulem, P. L. Sulem and H. Frisch, "Tracing complex singularities with spectral methods", *J.* Comp. Phys. **50**, 138–161, (1982).

[17] T. Matsumoto, J. Bec and U. Frisch, "Complex–space singularities of 2D Euler flow in Lagrangian coordinates", *Physica D* **237**, 1951–1955, (2008).

[18] M. Siegel and R. E. Caflisch, "Calculation of complex singular solutions to the 3D incompressible Euler equations" *Physica D* **238**, 2368–2379, (2009).

[19] C. Bardos, U. Frisch, W. Pauls, S. S. Ray and E. R. Titi, "Entire Solutions of Hydrodynamical Equations with Exponential Dissipation", *Communications in Mathematical Physics* **293**, 519–543, (2010).

[20] H.-O. Kreiss and J. Lorenz, *Initial–Boundary Value Problems and the Navier–Stokes Equations*, SIAM, (2004).

[21] C. R. Doering, private communication, (2010).

[22] A. Ruszczyński, *Nonlinear Optimization*, Princeton University Press, (2006).

[23] M. D. Gunzburger, "Perspectives in flow control and optimization", SIAM, Philadelphia, (2003).

[24] J. Nocedal and S. J. Wright, *Numerical Optimization*, Springer Series in Operations Research, (1999).

[25] E. M. Stein and R. Shakarchi. *Real Analysis. Measure Theory, Integration and Hilbert Spaces*, Princeton University Press, 2005.

[26] B. Protas, T. Bewley and G. Hagen, "A comprehensive framework for the regularization of adjoint analysis in multiscale PDE systems", *Journal of Computational Physics* **195** (1), 49-89, (2004).

[27] B. Protas, "Adjoint–based Optimization of PDE Systems with Alternative Gradients", *Journal of Computational Physics*, 2008.

[28] W. H. Press, B. P. Flannery, S. A. Teukolsky and W. T. Veterling, *Numerical Recipes*, Cambridge University Press, 1986.

[29] D. Ayala, *Maximum Enstrophy Growth in Burgers Equation*, M.Sc. Thesis, McMaster University, (2010).

[30] R. Dascaliuc, C. Foias and M. S. Jolly, "Estimates on enstrophy, palinstrophy, and invariant measures for 2-D turbulence", *J. Differential Equations* **248**, 792–819, (2010).

[31] T. R. Bewley, P. Moin and R. Temam, "DNS–based predictive control of turbulence: an optimal benchmark for feedback algorithms", *J. Fluid Mech.* **447**, 179–225, (2001).

[32] M. Farazmand, N. K. R. Kevlahan and B. Protas, "Controlling the dual cascade of two–dimensional turbulence", *J. Fluid Mech.* **668**, 202–222, (2011).